Kinetics and mechanism of natural fluorapatite dissolution at 25°C and pH from 3 to 12

Claire Chaïrat[1,2], Jacques Schott[1], Eric H. Oelkers[1], Jean-Eric Lartigue[2] and Najatte Harouiya[1]

1- *Géochimie et Biogéochimie Expérimentale, LMTG/CNRS UMR 5563/Université Paul Sabatier 14 av. Edouard Belin 31400 Toulouse France*

2- *Laboratoire d'étude du Comportement à Long Terme LCLT/SECM/DTCD CEA Valrhô BP17171 30207 Bagnols-sur-Cèze Cedex France*

Corresponding author: Eric H. Oelkers Géochimie et Biogéochimie Expérimentale LMTG/CNRS UMR 5563/Université Paul Sabatier 14, av. Edouard Belin 31400 Toulouse France

e-mail: oelkers@lmtg.obs-mip.fr

Abstract : The dissolution rates of natural fluorapatite (FAP) $Ca_{10}(PO_4)_6F_2$ were measured at 25°C in mixed-flow reactors as a function of pH from 3.0 to 11.7, and aqueous calcium, phosphorus, and fluoride concentration. After an initial preferential Ca and/or F release, stoichiometric Ca, P, and F release was observed. Measured FAP dissolution rates decrease with increasing pH at $3 \le pH \le 7$, FAP dissolution rates are pH independent at $7 \le pH \le 10$, and FAP dissolution rates again decrease with increasing pH at $pH \ge 10$. Measured FAP dissolution rates are independent of aqueous Ca, P and F concentration at $pH \approx 3$ and $pH \approx 10$.

Apatite dissolution appears to be initiated by the relatively rapid removal from the near surface of F and the Ca located in the M1 sites, via proton for Ca exchange reactions. Dissolution rates are controlled by the destruction of this F and Ca depleted surface layer. The destruction of this layer is facilitated by the penetration of protons into the surface at acidic conditions, and by surface hydration at neutral and basic conditions. Taking into account these two parallel mechanisms, measured fluorapatite forward dissolution rates can be accurately described using:

$$r_+(\text{mol m}^{-2}\ \text{s}^{-1}) = 6.61\times10^{-6}\frac{(a_{H^+})K_{ads}}{1+(a_{H^+})K_{ex}+\dfrac{(a_{Ca^{2+}})^4(a_{F^-})^{1.4}(a_{OH^-})^{0.6}}{(a_{H^+})^6K_{ex}}} + 3.69\times10^{-8}[\equiv CaOH_2^+]^{0.6\pm0.1}$$

where a_i refers to the activity of the i^{th} aqueous species, $[\equiv CaOH_2^+]$ denotes the concentration of hydrated calcium sites at the surface of the leached layer (mol m^{-2}), and K_{ex} and K_{ads} stand for the apparent stability constants of the Ca^{2+}/H^+ exchange and adsorption/penetration reactions, respectively.

Keywords: apatite, fluorapatite, surface reactivity, dissolution, kinetic, mechanism

1. INTRODUCTION

Until recently the majority of research on apatite dissolution kinetics focused on human health applications (White and Nancollas, 1977; Budz and Nancollas, 1988; Chin and Nancollas, 1991; Chin et al., 1993; Christoffersen et al., 1998). Comparatively few studies were devoted to the dissolution kinetics of the geologically abundant fluorapatite (FAP) at geologically relevant conditions. Valsami-Jones et al. (1998) investigated the influence of aqueous Cd and Pb on apatite dissolution at 25°C and pH 2 to 7; Welch et al. (2002) investigated the effect of microorganisms and microbial metabolites on apatite dissolution; and Guidry and Mackenzie (2003) measured the dissolution rates of fluorapatite and carbonate fluorapatite as a function of temperature, solution saturation state, and pH from 2 to 8.5. Dorozhkin (1997) investigated the reactions at the surface of apatite briefly exposed to 2–7 mol/L H_3PO_4 solutions. This author proposed a mechanism for FAP dissolution at acidic conditions. The present study aims to build upon this past work toward an improved understanding of FAP surface reactivity. The first paper in this series described the chemistry of the fluorapatite-solution interface as a function of pH (Chaïrat et al., 2006 b). In this second paper we report measured FAP dissolution rates at 25°C for a wide range of pH and solution compositions. These data are used together with transition state theory to generate rate equations describing FAP dissolution kinetics in natural aquatic systems.

2. THEORETICAL CONSIDERATIONS

The standard state adopted in this study is that of unit activity for pure minerals and H_2O at any temperature and pressure. For aqueous species other than H_2O, the standard state is unit activity of the species in a hypothetical 1 molal solution referenced as infinite dilution at any temperature and pressure. All thermodynamic calculations in the present study, including calculation of mineral saturation states, were performed using PHREEQC (Parkurst, 1998) together with its llnl database (Johnson et al., 2000).

The FAP dissolution can be expressed as

$$Ca_{10}(PO_4)_6F_2 = 10\ Ca^{2+} + 6\ PO_4^{3-} + 2\ F^- \quad (1)$$

The law of mass action for reaction (1) is given by

$$K_s = (a_{Ca^{2+}})^{10}(a_{PO_4^{3-}})^6(a_{F^-})^2 \quad (2)$$

where K_S refers to the equilibrium constant for reaction (1) and a_i denotes the activity of the i^{th} aqueous species.

Mineral dissolution and crystallization rates can be described via transition state theory (TST). According to TST, the overall rate r of a mineral dissolution reaction can be depicted using (Lasaga, 1981; Aagard and Helgeson, 1982):

$$r = r_+\left(1 - \exp\left(-\frac{A}{\sigma RT}\right)\right) \quad (3)$$

where r_+ designates the forward dissolution rate per unit surface area, A stands for the chemical affinity of the overall dissolution reaction, R denotes the gas constant and σ stands for Tempkin's average stoichiometric number equal to the ratio of the rate of destruction of the activated complex relative to the overall dissolution rate. The parenthetical term in Eqn. (3) takes into account the effect of the back reaction as equilibrium is approached and insures that $r=0$ at equilibrium. The chemical affinity is defined as:

$$A = -RT \ln\left(\frac{Q}{K_s}\right) = -2.303RT\mathrm{Log}(\Omega) \quad (4)$$

where Q refers to the reaction activity quotient, and Ω represents the saturation index ($\Omega = Q/K_s$). The form of Eqn. (3) is such that overall rate (r) equals forward rate (r_+) when $A >> \sigma RT$, but decrease continuously to 0 at equilibrium with decreasing A when $A < \sigma RT$.

The forward reaction rate (sometimes referred to as the far from equilibrium rate), r_+, is equal to the product of two factors, the concentration of a rate-controlling surface species called the precursor complex ($P^{\#}$), and the rate of destruction of this complex to form the reactions products (Wieland et al., 1988; Stumm and Wieland, 1990; Oelkers et al., 1994). This concept is consistent with:

$$r_+ = k_{P^{\#}}[P^{\#}] \quad (5)$$

where $k_{P^{\#}}$ refers to the rate constant for the decomposition of $P^{\#}$ into products, and $[P^{\#}]$ stands for its concentration. The application of Eqn. (5) to describe FAP dissolution requires knowledge of the precursor complex identity and formation reactions.

The precursor complex is formed by removing or adding material to the mineral surface. A general reaction for precursor complex formation is given by:

$$\text{Mineral} + \sum_i n_i X_i = \text{Precursor} \quad (6)$$

where n_i signifies stoichiometric coefficients, and X_i represents a species in the precursor forming reaction. Note this reaction may involve some combination of sorption and exchange reactions (c.f. Oelkers, 2001). The law of mass action for the creation of the precursor complex can be written:

$$[P^{\#}] = \frac{K^{\#} \prod_i \frac{a_i^{n_i}}{\gamma^{\#}}}{1 + K^{\#} \prod_i \frac{a_i^{n_i}}{\gamma^{\#}}} \quad (7)$$

where $\gamma^{\#}$ denotes the activity coefficient of the precursor complex, a_i stands for the activity of the subscripted species, and $K^{\#}$ symbolizes the equilibrium constant for reaction (6). It follows from Eqns. (5) and (7) that the precursor complex and its formation reaction can be determined from the variation of r_+ as a function of solution composition. This exercise will be performed in the present study by measuring FAP dissolution rates at far from equilibrium conditions as a function of pH and aqueous Ca, P, and F concentration.

3. MATERIALS AND METHODS

3.1. Fluorapatite samples

Natural pegmatitic fluorapatite from Paraïba, Brazil was used in this study. X-ray diffraction analysis of this sample shows it is well crystallized, pure apatite. The composition of this apatite was found to be consistent with $Ca_{10.0}(PO_4)_{6.0}F_{1.4}(OH)_{0.6}$ (see Chaïrat et al., 2006 b). The sample was initially crushed with a hammer covered by a plastic sheet then ground with an agate mortar and pestle and sieved. The 113-200 μm size fraction was cleaned ultrasonically 10 times with alcohol. Scanning Electron Microscope (SEM) images show the resulting powder to be essentially free of fine particles; a representative SEM image of this cleaned powder is provided in Fig. 1. The BET surface area of this powder as determined by eight point krypton adsorption using a Micrometrics ASAP 2010 is 1263±10% cm^2/g.

3.2. Dissolution rates measurements

Dissolution rates were measured in open-system, mixed-flow reactors consisting of 120 ml Savillex® fusion vessels placed in a 25°C thermostated room (e.g. Köhler et al., 2005). These reactors were fitted with Nalgene® tubes for inlet and outlet fluid passage. Dissolution experiments were initiated by placing from 0.18 to 3.9 g of FAP powder into the reactors. The reactors were then filled with inlet solution, sealed, and the reactor attached to the inlet and outlet solution lines. The inlet solution was pumped into the reactors at a constant rate with Gilson® peristaltic pumps; all outlet fluids passed through a 0.45 μm Millipore® Nitrocellulose filter while exiting the reactors. Mounted teflon coated stirring bars rotated at 150 to 250 rpm mixed the fluid-mineral powder slurry while avoiding grinding. Outlet solutions were collected regularly for analysis. All experiments were performed in solutions having an ionic strength fixed at 10^{-2} M by adding appropriate quantities of NaCl or NH_4Cl, and the solution pH was fixed by adding reagent grade HCl, NaOH, or NH_4OH. Solutions

containing calcium, phosphorus, or fluoride were prepared by addition of $Ca(NO_3)_2$, $K(H_2PO_4)$ or NaF, respectively. Steady-state rates were determined from outlet solution Ca, P, and F concentration. Steady-state was typically attained after four residence times, and is defined by outlet solution compositions that are constant, within analytical uncertainty, for at least three additional residence times. The residence time is defined as the reactor volume divided by the fluid flow rate. For each experiment, at least four data points at steady-state conditions were collected. FAP dissolution rates were computed from measured steady-state outlet solution Ca, P, and F concentrations using:

$$r_i = \frac{([i]_{out} - [i]_{in})F}{\nu_i S} \quad (8)$$

where r_i refers to the dissolution rate based on the release rate of the i^{th} element, $[i]_{out}$ and $[i]_{in}$ stand for the outlet and inlet concentration of the i^{th} element respectively, F represents the fluid flow rate, ν_i denotes a stoichiometric coefficient of the i^{th} element in one mole of FAP, and S denotes the total FAP surface area present in the reactor. S was calculated by multiplying the mass of powder in the reactor by the powder's initial specific BET surface area. Uncertainties on steady-state rates are 15-30% and are dominated by the uncertainty on BET surface area measurements (±10%).

Outlet solution pH was measured at 25° C within a few hours of sampling using a Metrohm© 744 pH meter coupled to a Metrohm© Pt1000/B/2 electrode with a 3 M KCl outer filling solution. The electrode was calibrated with NBS standards at pH 4.01, 6.86, 9.22, and 11.00 with an average error less than 0.05 pH units. Calcium concentrations were measured by flame atomic absorption spectroscopy using a Perkin Elmer® 5100 with a detection limit 0.3ppm and a precision of better than 4%. Fluoride and phosphate analyses were performed with a Dionex High Pressure Liquid Chromatography (HPLC) after elimination of chloride

ions using DIONEX® Onguard II $AgNO_3$ cartridges with a detection limit of 0.1 and 0.3ppm, respectively, and a precision of better than 8%.

4. RESULTS

4.1. Stoichiometry of fluorapatite dissolution

All FAP open system dissolution experiments exhibited a similar initial temporal outlet solution evolution. An example of this evolution is shown in Figs. 2 and 3. During the initial part of each experiment, molar Ca/P and F/P ratios of the outlet fluids exceed those of the dissolving apatite before a steady-state is attained where Ca and F are in stoichiometric proportions relative to P.

4.2. pH dependence of fluorapatite dissolution rates

Fluorapatite dissolution rates obtained in the present study are listed in Table 1 and illustrated in Figs. 4 and 5. Consistent with the relative stoichiometry discussed above, steady-state dissolution rates based on calcium, phosphorus or fluoride release were found equal within the experimental uncertainty which confirms that FAP dissolution is stoichiometric. Note that at alkaline conditions, FAP dissolution rates calculated from fluoride analyses are slightly higher than those computed from calcium measurements but this effect stems mostly from the analytical uncertainties; fluoride concentrations in these experiments are near the analytic limit detection. The rates depicted in Fig. 5 are based on Ca outlet solution concentration which has lower uncertainty than corresponding rates based on F and P release. For comparison, FAP dissolution rates reported by Valsami-Jones et al. (1998) and Guidry and Mackenzie (2003) are also shown in the same figure. Dissolution rates measured in this study are closely consistent with values reported by Guidry and Mackenzie (2003). In contrast, the dissolution rate reported by Valsami-Jones et al. (1998) at I=0.1M and pH=5.2, is somewhat faster than the corresponding rates determined in the present study. This discrepancy could be due to a number of factors including differences in the reactor types used in the two studies, or differences in reactive fluid compositions.

The pH dependence of dissolution rates exhibits three distinct slopes. At $pH \leq 7$, fluorapatite dissolution rates apparently decrease monotonically with increasing pH. The logarithm of dissolution rates versus pH decreases linearly with pH with a slope ~-0.9 which is close to that reported by Guidry and Mackenzie (2003); this observation suggests a rate equation of the form:

$$r = k(a_{H^+})^n \quad (9)$$

where k denotes the rate constant ($k=6.61 \times 10^{-6}$ mol m^{-2} s^{-1}), and $n=0.9$ describes a reaction order with respect to protons. At $7 \geq pH \geq 10$, FAP dissolution rates appear to be pH independent. This variation was also suggested by Guidry and Mackenzie (2003). At $pH \geq 10$, measured FAP dissolution rates decrease with increasing pH with a slope of about -0.5.

The saturation state of all steady-state outlet solutions with respect to the potential secondary phases listed in Table 2 are reported in Table 3; they indicate that the solutions were undersaturated with respect to all considered solid phases at acidic conditions. The outlet solutions were found to be supersaturated with respect to igneous hydroxyapatite (HAP) and β tri calcium phosphate (β-TCP) during some experiments performed in alkaline conditions (e.g. FAP17-FAP22). However, neither igneous HAP or β-TCP are observed to form at low temperature (Vieillard and Tardy, 1984; Lacout, 2005 personal communication) and the stoichiometric release of Ca relative to P and F observed at steady-state conditions suggest that precipitation of these phases did not occur during the experiments. At alkaline pH, despite FAP dissolution occurs, outlet solution were found to be supersaturated with respect to this mineral (see Table 4). However, it has been shown in the first part of this study (Chaïrat et al., 2006 b) that a leached layer of di-calcium phosphate stoichiometry formed at the FAP surface during its dissolution and controlled the mineral solubility. The outlet fluid Ca/P and F/P ratio suggest this layer formed during the initial dissolution of FAP before steady-state was attained. The steady-state outlet solution saturation state with respect to di-

calcium phosphate was evaluated using the Log(K_s) reported for this leached layer by Chaïrat et al. (2006 b). Results of these calculations, which are presented in Table 4, indicate that all but five of the dissolution experiments performed in this study were at far from equilibrium ($A \geq 2.5 kJ/mol$) with respect to this leached layer. Moreover, dissolution rates measured for the experiments performed closer to equilibrium ($1.8 \leq A \leq 2.3 kJ/mol$) were the same within uncertainties than those performed far form equilibrium at the same pH. The surface of FAP after the dissolution experiments was examined by SEM. Several representative SEM images are shown in Fig. 1. FAP dissolved at acid conditions exhibit etch pit formation, whereas little change was observed on the surfaces of apatite dissolved at alkaline conditions.

4.3. The effect of solution composition on fluorapatite dissolution rates

FAP forward dissolution rates were measured in presence of calcium, fluoride, and phosphorus at both acidic and basic conditions. Results are listed in Table 5 and illustrated in Fig. 6. It can be seen that FAP dissolution rates are found to be independent of aqueous calcium, phosphate, and fluoride activity in both acidic and basic solutions.

5. FLUORAPATITE DISSOLUTION MECHANISM

The experimental observations presented above and crystallographic considerations help illuminate the fluorapatite dissolution mechanism. The variation of FAP dissolution rates with pH exhibits a break in slope at near neutral conditions. Such slope breaks have been observed for other minerals such as olivines (Pokrovsky and Schott, 2000) and carbonates (Pokrovsky and Schott, 1999; Pokrovsky et al. 1999) where it has been correlated with the corresponding surface concentration of H^+, $\equiv CaOH_2^+$ or $\equiv MgOH_2^+$.

The FAP structure consists of individual phosphate tetrahedra linked by calcium atoms. The phosphate groups forms the skeleton having two types of metal sites. The first (M1 site) is occupied by four calcium atoms that have a 9-fold coordination, while the second (M2 site) is occupied by six calcium atoms having a 7-fold coordination. Fluoride anions are located within the same channels as the M2 sites and have a high mobility. The FAP structure thus contains Ca-F, Ca-O and P-O bonds; consideration of the relative electrostatic strength of these bonds suggests that their relative destruction rate is consistent with: Ca-F > Ca(1) -O > Ca(2)-O > P-O. Considering its structure, once all Ca-F, and Ca-O bonds are broken, FAP is destroyed; the breaking of P-O bonds are unnecessary for FAP dissolution. This suggests that the FAP dissolution behavior may be similar to that of olivine, which is also constituted of isolated SiO_2 tetrahedra, and whose dissolution has been attributed to two distinct mechanisms, one dominating at acidic and one dominating at alkaline conditions (Pokrovsky and Schott, 2000). Adopting a similar approach, the mechanisms of FAP dissolution at these two conditions are considered below.

5.1. Neutral and basic solutions

A fluoride depleted layer forms at the FAP surface in basic solutions. This fluoride depletion is confirmed by XPS data (Chaïrat et al., 2006 b) and the initial preferential departure of fluoride from FAP surface during dissolution experiments. Surface titrations of the FAP suggest that fluoride removal is coupled to the penetration of hydroxide consistent with an ion exchange mechanism (Chaïrat et al., 2006 b). This exchange is supported by the similar location of hydroxyl and fluoride ions in apatite structure, and by existence of a solid-solution between FAP and hydroxyapatite (HAP) (Schaeken et al., 1975). However, attenuated total reflectance spectroscopy (ATR) suggests that some F removal is coupled to a concurrent removal of Ca (Chaïrat et al., 2006 b). Although the site from which this removed Ca originates has not been experimentally identified, the relative coordination of each cation suggests that calcium atoms located in M1 sites are easier to remove than those located in the M2 sites. Nevertheless, FAP dissolution is controlled by the breaking of Ca-O bonds; by analogy with the alkaline dissolution mechanism of oxides (Stumm, 1992; Pokrovsky and Schott, 2004), carbonate minerals (Pokrovsky and Schott, 1999) and some basic silicates (Pokrovsky and Schott, 2000), the breaking of Ca-O bonds is promoted by the hydratation of surface calcium. As is the case for oxides, silicates, and carbonates, calcium at apatite surface is present in acid to weakly alkaline conditions as $\equiv CaOH_2^+$. This site loses a proton in strongly alkaline solutions according to:

$$\equiv CaOH_2^+ \rightarrow \equiv CaOH^0 + H^+ \qquad K_{int(10)} \qquad (10)$$

where $K_{int(10)}$ refers to the surface intrinsic stability constant of reaction (10). The law of mass action for reaction (10) has been used together with the non electric double layer model incorporated in the FITEQL 3.2 code (Herbelin and Westal, 1996) to fit surface titration data of Chaïrat et al. (2006 b). This fit yielded $\log(K_{int(10)}) = -10$ and a total calcium surface site concentration of 3.2 µmol/m². The intrinsic stability equilibrium constant for reaction (10) is

close to the corresponding values proposed for the calcite and dolomite surface (Pokrovsky et al., 1999; Fenter et al. 2000; Pokrovsky and Schott, 2001; 2002). The total number of calcium surface sites concentration is, however, about 65% lower than that determined by Wu et al. (1991) from FAP crystallographic data.

The evolution of $\equiv CaOH_2^+$ and $\equiv CaOH$ site concentrations as a function of pH is illustrated in Fig. 7. FAP dissolution rates measured in neutral and alkaline solution in this work and those reported by Guidry and Mackenzie (2003) are also shown in this figure to demonstrate the close correspondence between $\equiv CaOH_2^+$ concentration and FAP dissolution rates. At $pH \leq 10$, nearly all Ca surface sites are protonated and dissolution rates are pH independent. At $10 \leq pH \leq 12$, $[\equiv CaOH_2^+]$ decreases with increasing pH in a manner similar to measured FAP dissolution rates. This suggests FAP dissolution rates at these conditions can be described using:

$$r_b = k_b \cdot [\equiv CaOH_2^+]^c \qquad (11)$$

where k_b designates a rate constant, $[\equiv CaOH_2^+]$ refers to the concentration of protonated surface calcium sites, and c stands for a reaction order with respect to these sites concentration. The rate constant, k_b, and reaction order, c, can be determined by plotting the logarithm of neutral and basic dissolution rates as a function of the logarithm of $[\equiv CaOH_2^+]$. This regression was performed with the aid of Fig. 8. The slope and intercept of the regression curve yields $c \approx 0.6$ and $k_b \approx 3.69 \times 10^{-8}$ mol s^{-1} respectively.

5.2. Acidic solutions

An initial preferential release of Ca and F relative to P was observed during FAP dissolution in acidic solutions (see Fig. 2). ATR spectroscopy and solubility experiments suggest that the F and Ca removal is coupled to phosphate hydrolysis and leads to the formation of a di-calcium phosphate leached layer ($CaHPO_4$) (Chaïrat et al., 2006 b). The fact that we did not observe any effect of calcium and fluoride aqueous activities on FAP dissolution rates suggests that this step is rapid and 1) F removal from the FAP surface and 2) of Ca from the relevant Ca site is complete. The Ca/P ratio of the leached layer (~1) suggests that four calcium atoms are preferentially released from the FAP surface during its initial dissolution. This is consistent with crystallographic considerations that suggest that the four calcium atoms located in the M1 site are easier to remove than those located in the M2 site due to their relative coordination and interatomic distances. Note in addition that the preferential removal of 40% of calcium atoms site is also consistent with the calcium site surface concentration reported in this work and by Wu et al. (1991) (see above).

Combining these observations, a possible rate dissolution mechanism could consist of the initial irreversible coupled removal of the four Ca atoms located in the M1 site and all fluoride atoms located near the surface in accord with:

$$\equiv Ca_{10}(PO_4)_6F_{1.4}(OH)_{0.6} + 6\ H^+ \rightarrow \equiv Ca_6H_6(PO_4)_6 + 4\ Ca^{2+} + 1.4\ F^- + 0.6\ OH^- \qquad (12)$$

The law of mass action for this exchange reaction is given by:

$$K_{ex} = \frac{[\equiv Ca_6H_6(PO_4)_6]\cdot(a_{Ca^{2+}})^4\cdot(a_{F^-})^{1.4}(a_{OH^-})^{0.6}}{[\equiv Ca_{10}(PO_4)_6F_{1.4}(OH)_{0.6}]\cdot(a_{H^+})^6} \qquad (13)$$

where K_{ex} stands for the apparent stability constant of exchange reaction (12), a_i refers to the activity of the i^{th} aqueous species, and $[\equiv j]$ denotes the concentration of the j^{th} surface species.

The increase of FAP dissolution rates with decreasing pH at $pH \leq 7$ suggests that protons are involved in the acidic dissolution mechanism. Nevertheless, calcium sites are fully protonated in this range of pH (see above), and phosphate groups remain deprotonated at pH>1 (see Chaïrat et al., 2006 b). Protons involved in the dissolution mechanism are thus located elsewhere than in these surface sites. Spectroscopic analysis and potentiometric titrations showed that protons penetrate the apatite structure according to (Chaïrat et al., 2006 b):

$$\equiv Ca_6H_6(PO_4)_6 + n\ H^+ \rightarrow \equiv Ca_6H_{(6+n)}(PO_4)_6^{n+} \quad (14)$$

The law of mass action for this adsorption/penetration reaction is given by:

$$K_{ads} = \frac{[\equiv Ca_6H_{(6+n)}(PO_4)_6^{n+}]}{[\equiv Ca_6H_6(PO_4)_6] \cdot (a_{H^+})^n} \quad (15).$$

where K_{ads} stand for the apparent stability constant of reaction (14).

The protonated Ca and F depleted apatite constitutes the precursor complex. The final and limiting step of apatite dissolution is the destruction of the precursor complex by the hydrolysis of Ca-O bonds. In accord with TST, the forward FAP dissolution rate at acidic conditions, r_a, is proportional to the concentration of the precursor complex, such that:

$$r_a = k_a \cdot [\equiv Ca_6H_{(6+n)}(PO_4)_6^{n+}] \quad (16).$$

The concentration of $\equiv Ca_6H_{(6+n)}(PO_4)_6^{n+}$ can be determined combining Eqn. (13) and (15) with the conservation of surface site equation given by:

$$N = [\equiv Ca_{10}(PO_4)_6F_{1.4}(OH)_{0.6}] + [\equiv Ca_6H_6(PO_4)_6] + [\equiv Ca_6H_{(6+n)}(PO_4)_6^{n+}] \quad (17)$$

where N designates the total surface Ca site concentration, yielding:

$$r_a = k_a^{'} \frac{(a_{H^+})^n K_{ads}}{1 + (a_{H^+})^n K_{ex} + \frac{(a_{Ca^{2+}})^4 (a_{F^-})^{1.4} (a_{OH^-})^{0.6}}{(a_{H^+})^6 K_{ex}}} \quad (18)$$

with $k_a^{'} = N \cdot k_a$. Note that rate expression (18) is similar to that used by Brantley and Stillings (1996) to describe the dependence of feldspar dissolution rate on the surface concentration of protoned exchanged sites, that adopted by Oelkers and Schott (2001) to describe the dissolution rates of enstatite, and that proposed by Pokrovsky and Schott (2000) to describe forsterite dissolution at acidic conditions. In the case of forsterite, like for FAP, the magnesium release by Mg^{2+}/H^{+} exchange is followed by proton adsorption/penetration.

The description of FAP dissolution rates using Eqn. (18) requires four constants which can be deduced from the regression of experimental data. The slope and the intercept of the y axis of the straight line describing the logarithm of dissolution rates versus pH at $pH \leq 7$ yield $n \approx 1$ and $k_a^{'} \approx 6.61 \text{x} 10^{-6}$ mol m^{-2} s^{-1}, respectively. Assuming unit activity for mineral surface species, application of Eqn. (13) to the dissolution rates measured in presence of calcium and fluoride (e.g. experiments FAP23-FAP48) indicates that $K_{ex} \geq 10^{32}$. Lastly, the value of the apparent adsorption constant cannot be deduced directly by regression of experimental data and thus has been fixed to permit the best description of measured rates leading to $K_{ads} \approx 10^{(0.6 \pm 0.1)} \pm 15\%$. This value indicates that phosphate surface sites are deprotonated at acidic pH, which is consistent with the FAP iso electric point of 1 ± 0.5 reported by Chaïrat et al. (2006 b).

Combining the rate equations deduced for acidic and basic conditions leads to the following overall rate equation:

$$r = r_a + r_b = k_a^{'} \frac{(a_{H^+})^n K_{ads}}{1 + (a_{H^+})^n K_{ex} + \frac{(a_{Ca^{2+}})^4 (a_{F^-})^{1.4} (a_{OH^-})^{0.6}}{(a_{H^+})^6 K_{ex}}} + k_b \cdot [\equiv CaOH_2^+]^c \qquad (19).$$

The degree to which this equation can describe FAP dissolution rates may be assessed in Fig. 5, where the solid line depicts rates computed with Eqn. (19). The close correspondence between the curve and the experimental data demonstrates the consistency of measured rates

with Eqn. (19) and supports the hypothesis that FAP dissolution is controlled by two parallel reactions, the first predominating at acidic, and the second controlling the dissolution at neutral and basic conditions. Note that there is a slight discrepancy between calculated and experimental rates determined by Guidry and Mackenzie (2003) from pH 7 to 8.5 that may be due to the fact that these authors performed their experiments at higher ionic strength than that of this study (0.1M versus 0.01M).

6. CONCLUDING REMARKS

Results presented above illuminate the fluorapatite dissolution mechanism. The initial dissolution of FAP consists of the preferential removal of F and Ca. The final descruction of FAP results from the breaking of Ca-O bonds in the Ca and F depleted surface. The breaking of these bonds is facilitated by two distinct parallel reactions: 1) the adsorption/penetration of protons, which dominates at acid conditions and 2) the hydratation of the $\equiv CaOH_2^+$ complex at neutral and basic conditions. These distinct reactions lead to a pH variation of dissolution that exhibits slope breaks at a pH of ~ 7 and ~10.

This FAP dissolution mechanism, together with transition state theory allows development of a single rate equation that can describe accurately FAP dissolution over the full range of pH. The FAP mechanism and kinetic equations described above are independent of the nature of the anion located in the channel of apatite structure. It seems likely, therfore, that this same mechanism and equation can be applied to describe the dissolution rate of other apatite minerals including hydroxyapatite, chloroapatite, and apatite structured ceramics that could be effective radioactive waste storage hosts (e.g. Chaïrat et al., 2006 a).

REFERENCES

Aagaard P. and Helgeson H. C. (1982) Thermodynamic and kinetic constraints on reaction rates among minerals and aqueous solutions. I. Theoretical considerations. *Am. J. Sci.* **282**, 237–285.

Brantley S. L. and Stillings L. (1996) Feldspar dissolution at 25°C and low pH. *Am J. Sci.* **296**, 101-127.

Budz J. A. and Nancollas G. H (1988) The mechanism of dissolution of hydroxyapatite and carbonated apatite in acidic solutions. *J. Cryst. Growth.* **91**, 490–496.

Chaïrat C., Oelkers E. H., Schott J. and Lartigue J-E., (2006 a) An experimental study of the dissolution rates of Nd-britholite, an analogue of an apatite structured actinide bearing waste storage host. *J. Nucl. Mater.In press*.

Chaïrat C., Oelkers E.H., Schott J. and Lartigue J-E. (2006 b) A combined potentiometric, electrokinetic and spectroscopic study of fluorapatite surface composition in aqueous solutions and consequences on solubility properties. *Geochim. Cosmochim. Acta, submitted.*

Chin K. O. A. and Nancollas G. H. (1991) Dissolution of Fluorapatite. A constant-composition kinetics study. *Langmuir* **7**, 2175–2179.

Chin K. O. A., Johnsson M., Bergey E. J., Levine M. J. and Nancollas G. H. (1993) A constant composition kinetics study of the influence of salivary cystatins, statherin, amylase, and human serum albumin on Hydroxyapatite dissolution. *Coll. Surf. A: Physicochem. Eng. Asp.* **78**, 229–234.

Christoffersen M. R., Dohrup J., and Christoffersen J. (1998) Kinetics of growth and dissolution of calcium hydroxyapatite in suspensions with variable calcium to phosphate ratio. *J. Cryst. Growth.* **186**, 283–290.

Dorozhkin S. V. (1997) Acidic dissolution mechanism of natural fluorapatite II. Nanolevel of investigations *J. Cryst. Growth.* **182**, 133-140.

Fenter P., Geissbühler P., Dimasi E., Srajer G., Sorensen L. B. and Sturchio N. C. (2000) Surface speciation of calcite observed in situ by high-resolution X-ray reflectivity, *Geochimica et Cosmochimica Acta*, **64**, 1221-1228.

Guidry M. W. and Mackenzie F. T. (2003) Experimental study of ignous and sedimentary apatite dissolution: control of pH, distance from equilibrium, and temperature on dissolution rates *Geochim. Cosmochim. Acta* **67**, 2949-2963.

Herbelin A. L., Westall J. C. (1996), FITEQL version 3.2, a computer program for determination of chemical equilibrium constants from experimental data. Department of Chemistry, Oregon State University, Corvallis.

Johnson J., Anderson G. and Parkhurst D. (2000) Database from 'thermo.com.V8.R6.230' prepared by at Lawrence Livermore National Laboratory, (Revision: 1.11)

Kölher S. J., Harouiya N., Chaïrat C. and Oelkers E. H. (2005) Experimental studies of REE fractionation during water-mineral interactions: REE release rates during apatite dissolution from pH 2.8 to 9.2, *Chem. Geol*. **222**, 168-182.

Lasaga A.C. (1981) Transition State theory. *Rev. Min.* **8**, 135-169.

Oelkers E. H. (2001) General kinetic description of multioxide silicate mineral and glass dissolution *Geochim. Cosmochim. Acta* **65**, 3703-3719.

Oelkers E. H. and Schott J. (2001) An experimental study of enstatite dissolution and the mechanism of pyroxene/pyroxenoid dissolution. *Geochim. Cosmochim. Acta,* **65**, 1219-1231.

Oelkers E. H., Schott J., and Devidal J.-L. (1994) The effect of aluminum, pH, and chemical affinity on the rates of aluminosilicate dissolution reactions, *Geochim. Cosmochim. Acta* **58**, 2011-2024.

Parkhurst D. (1998) PHREEQC (Version 2)-A Computer Program for Speciation, Batch-Reaction, One Dimensional Transport, and Inverse Geochemical Calculations. http://wwwbrr.cr.usgs.gov/projects/GWC_coupled/phreeqc/index.html.

Pokrovsky O. S. and Schott J. (1999) Processes at the magnesium-bearing carbonates/solution interface. II. Kinetics and mechanism of magnesite dissolution. *Geochim. Cosmochim. Acta,* **63**, 881-897.

Pokrovsky O. S. and Schott J. (2000) Kinetics and mechanism of forsterite dissolution at 25°C and pH from 1 to 12. *Geochim. Cosmochim. Acta* **64**, 3313–3325.

Pokrovsky O. S. and Schott J. (2001) Kinetics and mechanism of dolomite dissolution in neutral to alkaline solution revisited. *Am. J. Sci.* **301**, 597-626.

Pokrovsky O. S. and Schott J. (2002) Surface chemistry and dissolution kinetics of divalent metal carbonates. *Environ. Sci. Technol.* **36**, 426-432.

Pokrovsky O. S. and Schott J. (2004) Experimental study of brucite dissolution and precipitation in aqueous solutions : surface speciation and chemical affinity control. *Geochim. Cosmochim. Acta* **68**, 31–45.

Pokrovsky O. S., Schott J. and Thomas F. (1999) Processes at the magnesium-bearing carbonates/solution interface. I. A surface speciation model for magnesite *Geochim. Cosmochim. Acta* **63**, 863-880.

Schaeken H. G., Verbeeck R. M. H., Driessens F. C. M and Thun H. P. (1975) Hydroxyapatite and Fluorapatite *Bull. Soc. Chim. Belges*., **84**, 881-890.

Stumm W. (1992) *Chemistry of the Solid–Water Interface. Wiley.*

Stumm W. and Morgan, J. J (1996) Aquatic chemistry, Chemical Equilibria and Rates In *Natural Waters Wiley-Interscience Publication*, 1022 p.

Stumm W. and Wieland E. (1990) Dissolution of oxide and silicate minerals: Rates depend on surface speciation. In *Aquatic Chemical Kinetics: Reaction Rates of Processes in Natural Waters (ed. W. Stumm)*, 367–400, *J. Wiley & Sons.*

Valsami-Jones E., Ragnarsdottir K. V., Putnis A., Bosbach B., Kemp A. J., and Cressey G., (1998) The dissolution of apatite in the presence of aqueous metal cations at pH 2–7. *Chem. Geol.* **151**, 215–233.

Viellard, P. and Tardy, Y. (1984) Thermochemical properties of phosphates. *In*: Niragu, J.O., Moore, P.B. (Eds.), *Phosphate Minerals*, 171–198, *Springer-Verlag, New York.*

Wagman (1982), NBS tables of chemical thermodynamic properties. *J. Phys. Chem.* Ref. Dat, **l1**1, Suppl 1.

Welch S. A., Tauton A. E. and Banfield J. F (2002) Effect of microorganisms and microbial metabolites on apatite dissolution, *Geomicrobiology Journal*, **19**, 343-367.

White W. and Nancollas G. H. (1977) Quantitative study of enamel dissolution under conditions of controlled hydrodynamics. *J. Dent. Res.* **56**, 524-530.

Wieland E., Wehrli B. and Stumm W. (1988) The coordination chemistry of weathering: III-Generalisation of dissolution rates of minerals. *Geochim. Cosmochim. Acta* **52**, 1969-1981.

Wu L., Willis F., and Schindler P. W. (1991) Surface complexation of calcium minerals in aqueous solution. *J. Coll. Inter. Sci.* **147**, 178-185.

FIGURE CONTENT

Figure 1: SEM photographs showing the surface of fluorapatite used in this study (a) before dissolution experiments, (b) after dissolution at 25°C and pH ≈ 4, and (c) after dissolution at 25°C and pH ≈ 10. Note the formation of etch pits in acid solutions (b) and the absence of secondary precipitation on alkaline solutions (c).

Figure 2: Outlet fluid composition evolution during a fluorapatite dissolution experiment at pH 4.5 and 25°C (experiment FAP3). Uncertainties on measured concentrations are approximately equal to the symbol size.

Figure 3: Temporal evolution of outlet fluid atomic Ca/P and F/P ratio during fluorapatite dissolution experiment at pH 4.5 and 25°C (experiment FAP3). The solid lines represent the corresponding ratios in the solid phase. The error bars on this figure correspond to a ±0.4 uncertainty on these ratios.

Figure 4: Logarithms of steady-state fluorapatite dissolution rates based on P (A) and F (B) release as a function of the corresponding rates based on Ca release. The solid line corresponds to stoichiometric dissolution of fluorapatite in accord with reaction (1). The error bars surrounding the data points in this figure correspond to the uncertainty in measured rates.

Figure 5: Logarithm of steady-state fluorapatite dissolution rates versus pH at 25°C and I=0.01M. The error bars surrounding the data points correspond to the uncertainty in measured rates. Similar error bars are attributed to the dissolution rates reported by Guidry and Mackenzie (2003). The solid line represents fit of experimental data with Eqn. (19) (see explanation in the text).

Figure 6: Logarithm of steady-state fluorapatite dissolution rates measured at 25°C as a function of corresponding aqueous activity at pH=3 (A) and pH=9 (B).

Figure 7: Comparison of fluorapatite dissolution rates and surface speciation at 25°C. The filled diamonds represent dissolution rates measured in this study and the open triangles correspond to rates reported by Guidry and Mackenzie (2003). The solid curves denote the relative concentration of the $[\equiv CaOH_2^+]$ (▬)and $[\equiv CaOH^0]$ (▬)surface species at the apatite surface quantified via the axis on the right hand side of the figure (see text).

Figure 8: Logarithm of fluorapatite dissolution rates measured at 25°C and $pH \geq 8$ as a function of the logarithm of concentration of the $\equiv CaOH_2^+$ surface species.

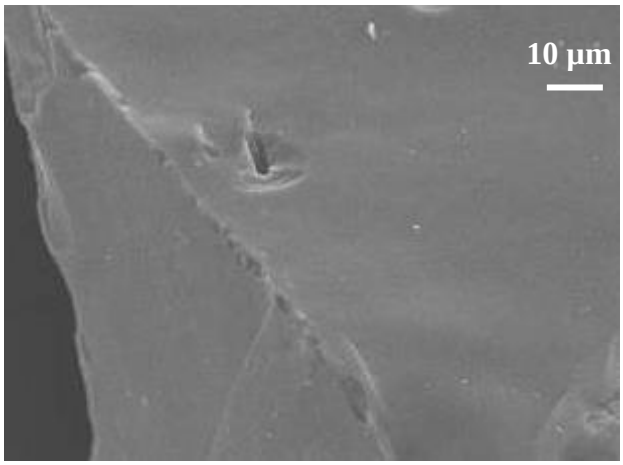

a

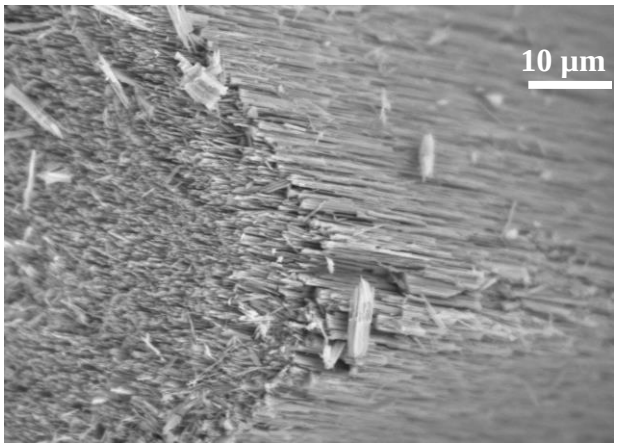

b

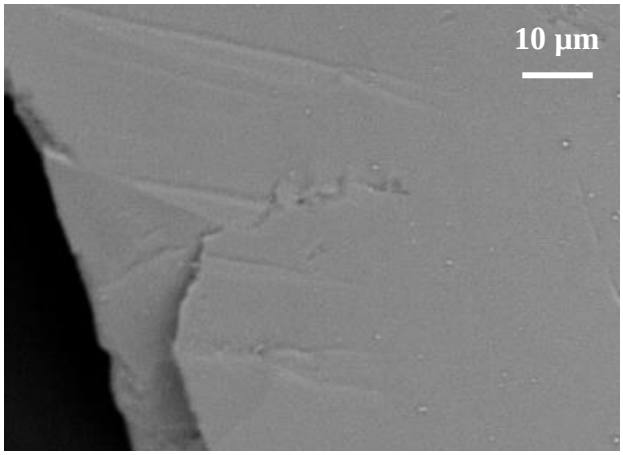

c

Figure 1

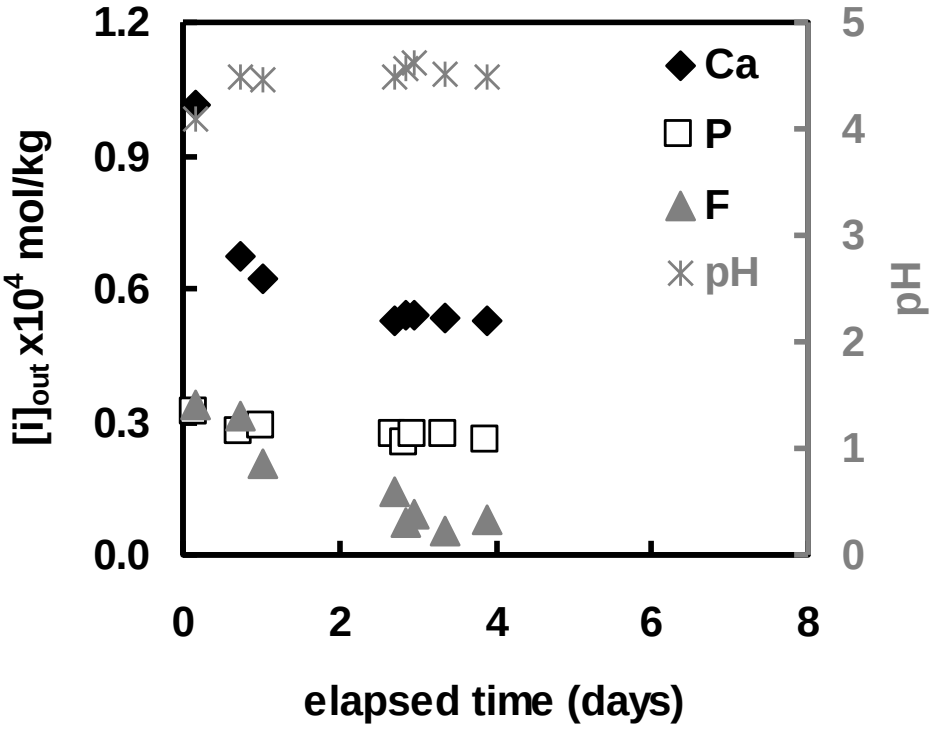
1.2
0.9
0.6
0.3
0.0
[i]out x10^4 mol/kg
0
2
4
6
8
elapsed time (days)
5
4
3
2
1
0
pH
Ca
P
F
pH

Figure 2

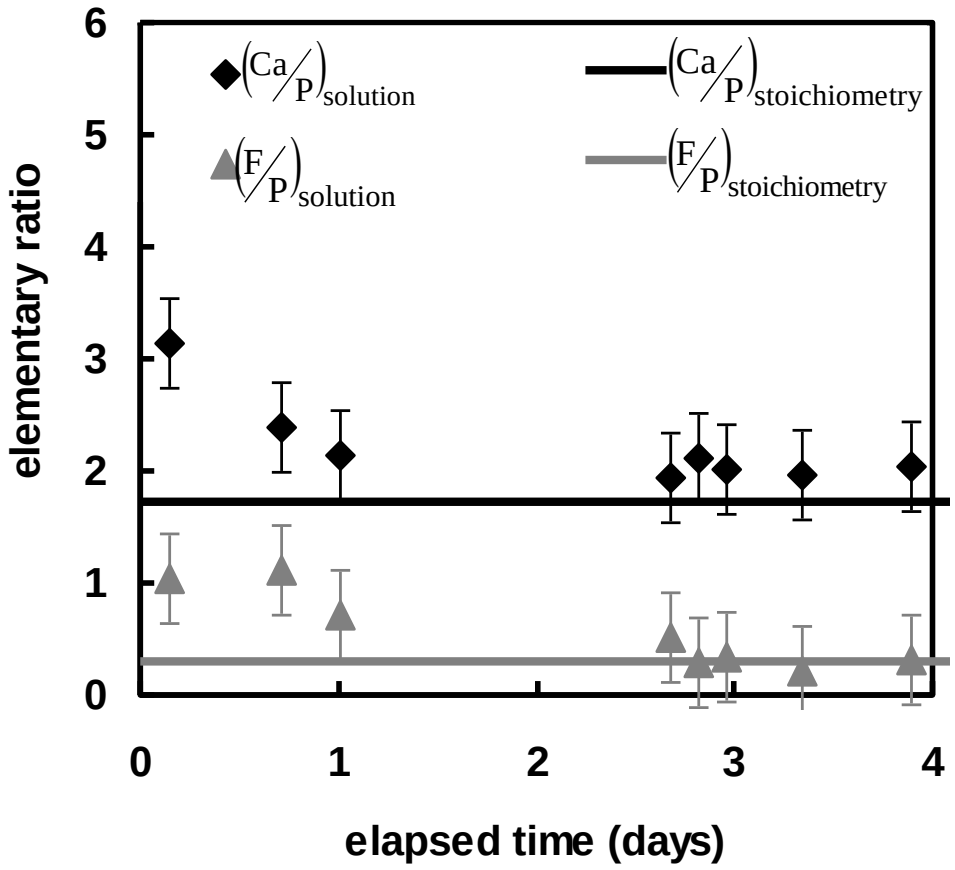
6
5
4
3
2
1
0
elementary ratio
(Ca/P)solution
(Ca/P)stoichiometry
(F/P)solution
(F/P)stoichiometry
0
1
2
3
4
elapsed time (days)

Figure 3

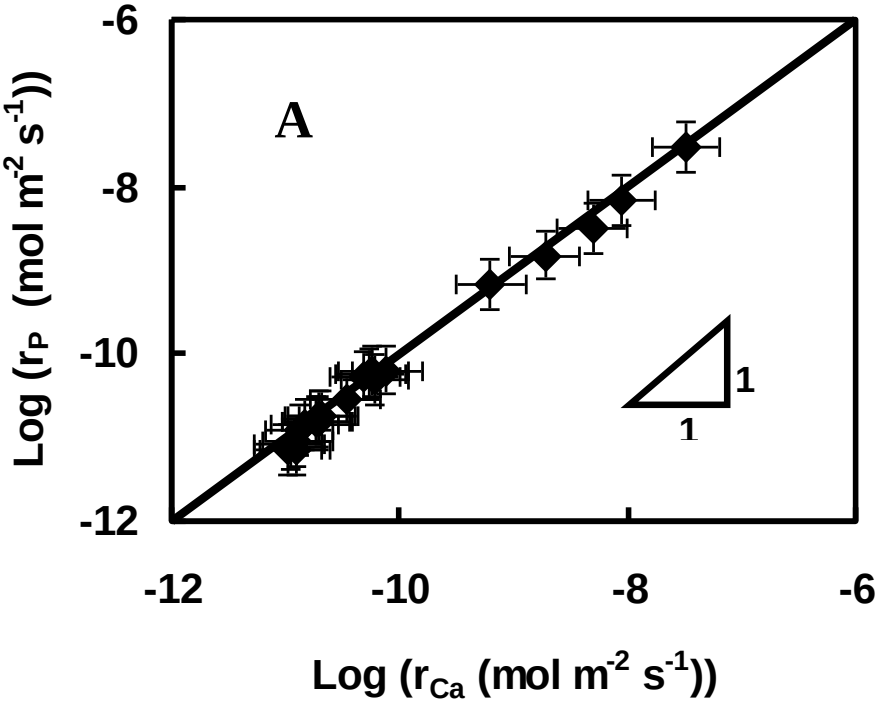
A
-6
-8
-10
-12
-12
-10
-8
-6
1
1
Log (r_P (mol m^{-2} s^{-1}))
Log (r_{Ca} (mol m^{-2} s^{-1}))

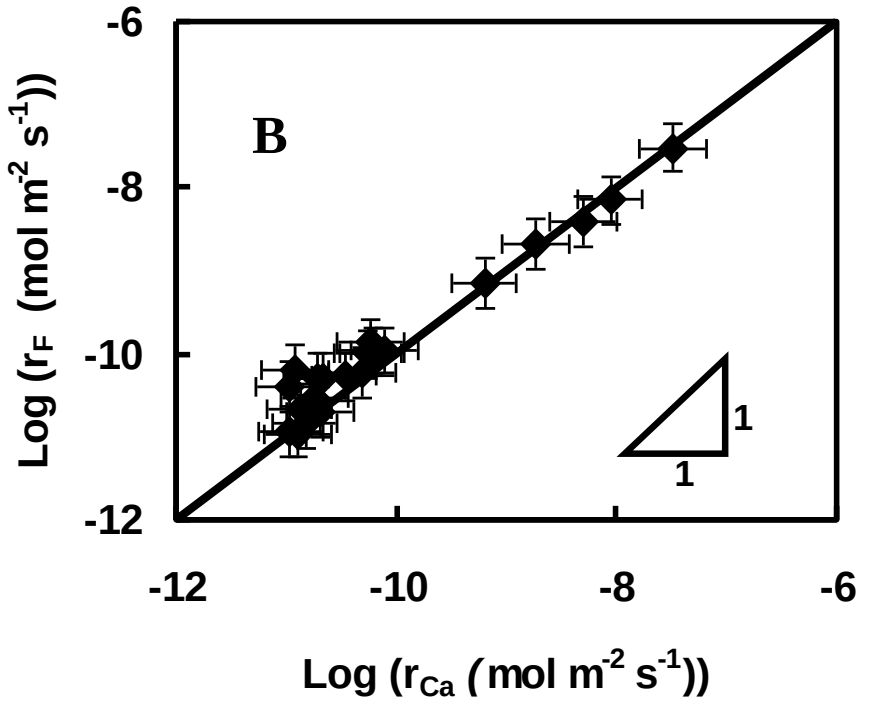
B
-6
-8
-10
-12
-12
-10
-8
-6
1
1
Log (r_F (mol m^{-2} s^{-1}))
Log (r_{Ca} (mol m^{-2} s^{-1}))

Figure 4

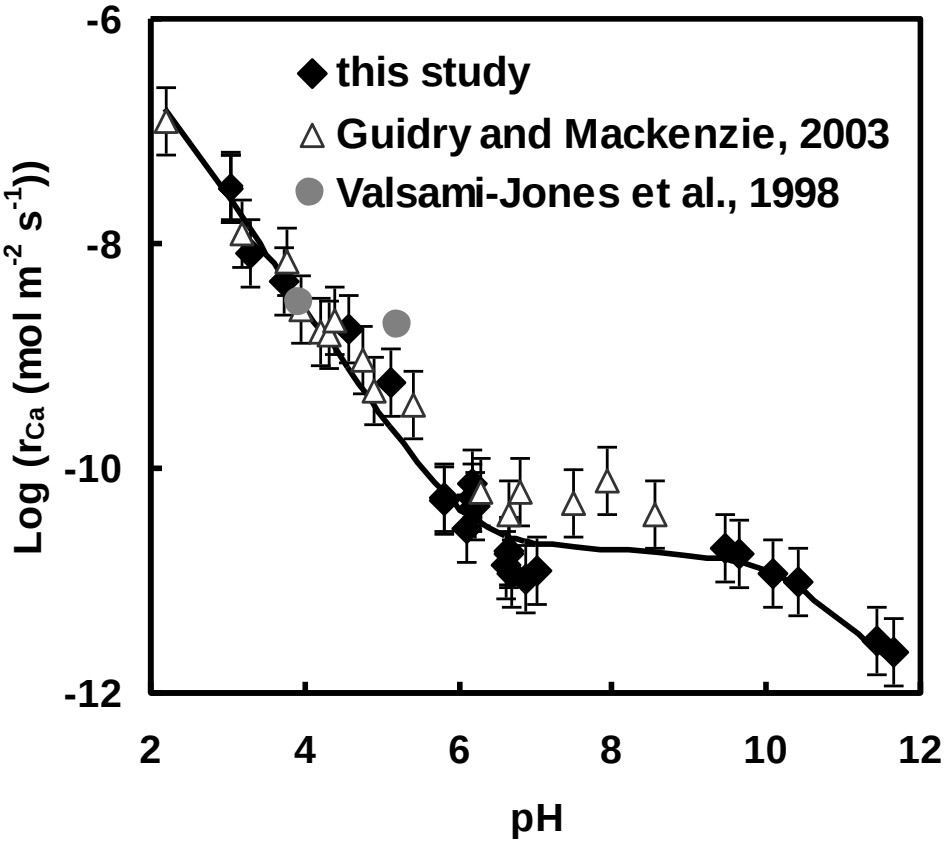
this study
Guidry and Mackenzie, 2003
Valsami-Jones et al., 1998
Log (rCa (mol m-2 s-1))
-6
-8
-10
-12
2
4
6
8
10
12
pH

Figure 5

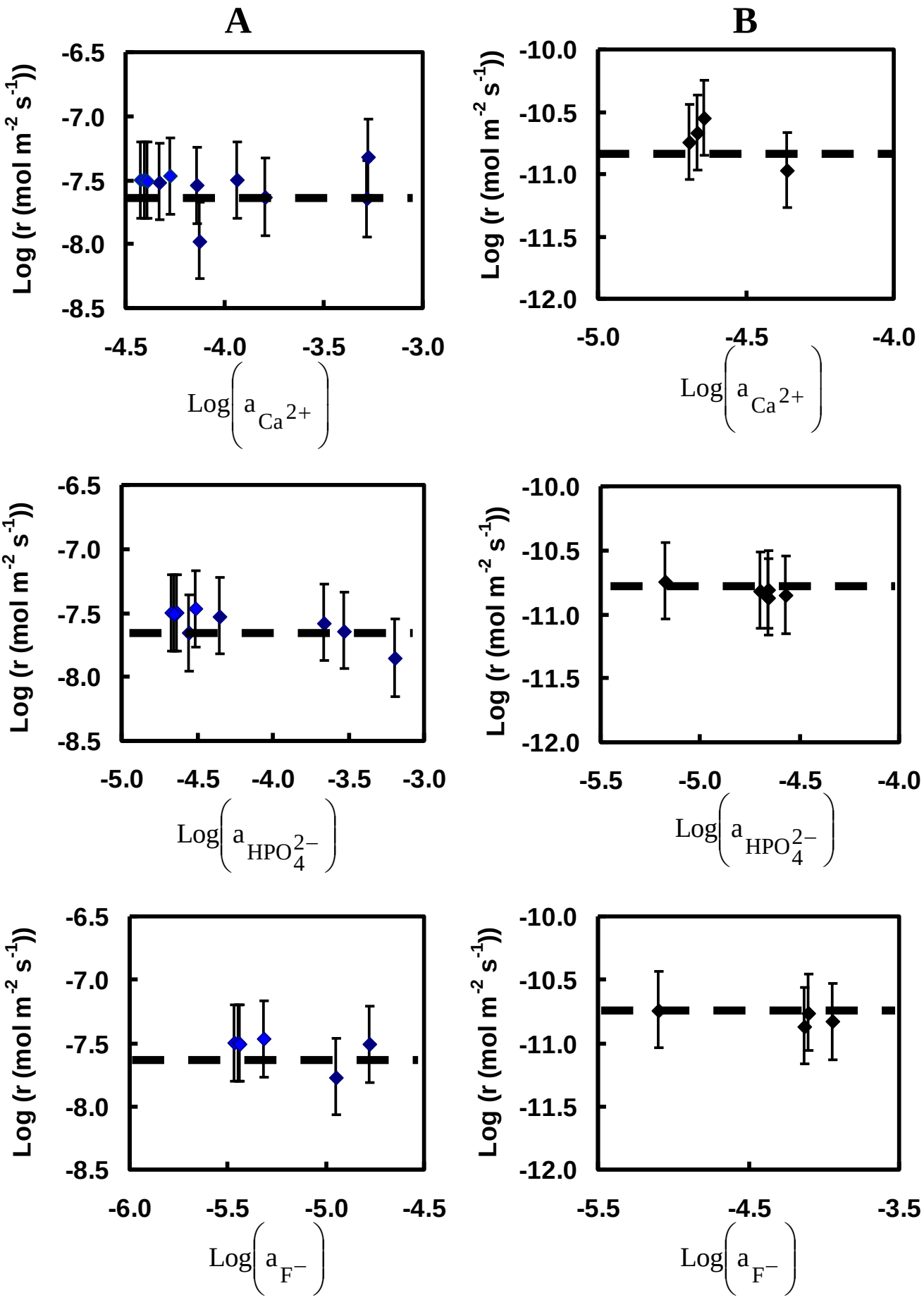
A
B
Log (r (mol m-2 s-1))
-6.5
-7.0
-7.5
-8.0
-8.5
-4.5
-4.0
-3.5
-3.0
Log (a Ca2+)
-10.0
-10.5
-11.0
-11.5
-12.0
-5.0
-4.5
-4.0
Log (a Ca2+)
-5.0
-4.5
-4.0
-3.5
-3.0
Log (a HPO42−)
-5.5
-5.0
-4.5
-4.0
Log (a HPO42−)
-6.0
-5.5
-5.0
-4.5
Log (a F−)
-5.5
-4.5
-3.5
Log (a F−)

Figure 6

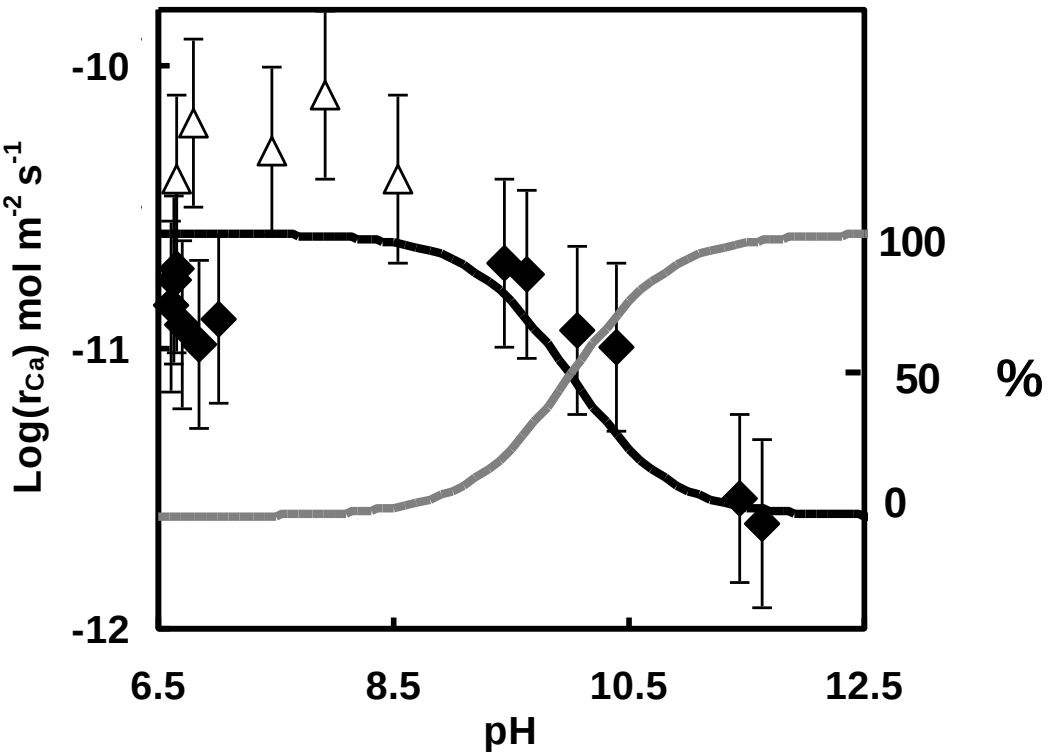

Figure 7

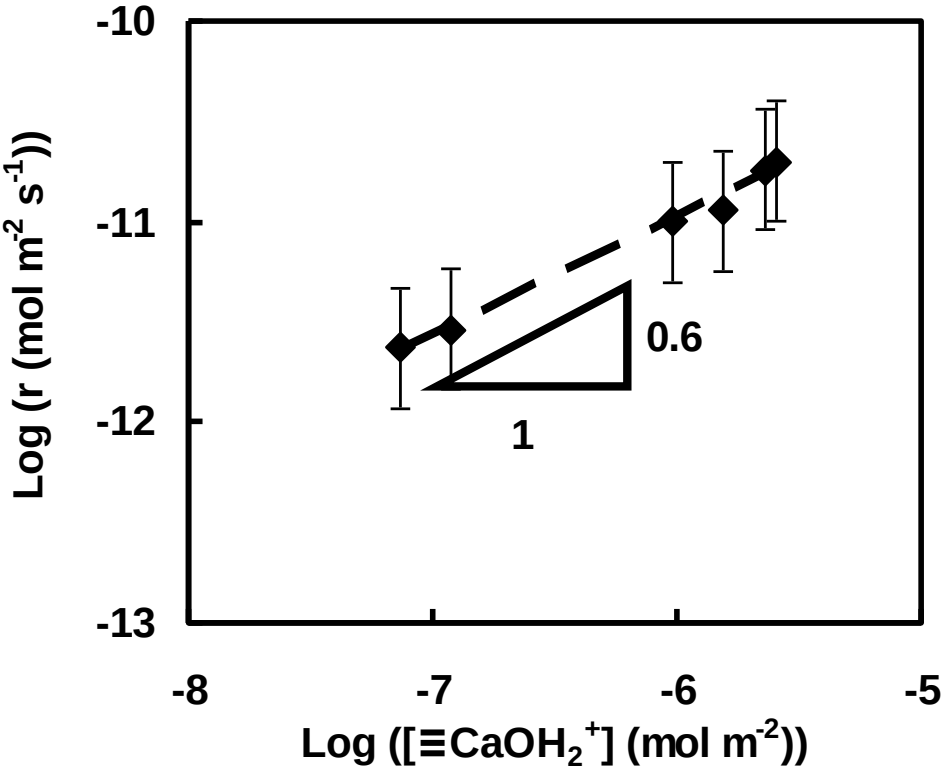

Figure 8

Table 1: Results of open-system fluorapatite dissolution experiments performed in the present study at 25°C.

Expt. number	Inlet solution composition	pH $_{inlet}$	pH $_{outlet}$	S	F	Steady-state outlet fluid concentration			Dissolution rates		
						$[Ca]_{out}$	$[P]_{out}$	$[F]_{out}$	Log(r_{Ca})	Log (r_P)	Log (r_F)
				cm²	mg s^{-1}		µmol kg^{-1}		Log(mol m^{-2} s^{-1})		
FAP0	HCl/NaCl	3	3.0	121	90.1	42.3	25.1	8.5	-7.50	-7.51	-7.50
FAP1	HCl/NaCl	3	3.3	289	7.2	344.6	162.9	40.6	-8.08	-8.16	-8.25
FAP2	HCl/NaCl	3.5	3.7	226	9.8	111.1	43.6	12.6	-8.33	-8.50	-8.51
FAP3	HCl/NaCl	4	4.5	218	7.5	53.7	26.5	9.1	-8.75	-8.82	-8.76
FAP4	HCl/NaCl	4.2	5.1	411	6	43.0	28.8	7.2	-9.22	-9.16	-9.24
FAP5	HCl/NaCl	4.9	5.8	1572	6.3	14.4	9.6	4.7	-10.24	-10.18	-9.97
FAP6	HCl/NaCl	5.3	5.8	1581	8	10.7	6.7	2.8	-10.27	-10.25	-10.03
FAP7	HCl/NaCl	5.6	6.1	1574	3.8	12.8	6.8	3.2	-10.52	-10.56	-10.36
FAP8	HCl/NaCl	5.3	6.2	1585	6.8	13.8	6.6	3.6	-10.24	-10.32	-10.07
FAP9	HCl/NaCl	5	6.2	1577	6.8	17.9	9.0	3.6	-10.12	-10.17	-9.96
FAP10	HCl/NaCl	6	6.2	1416	1.6	43.6	29.6	7.6	-10.33	-10.26	-10.33
FAP11	HCl/NaCl	5.6	6.6	1561	0.7	36.6	20.6	5.5	-10.85	-10.86	-10.92
FAP12	HCl/NaCl	5.3	6.6	1544	0.7	43.0	21.6	9.9	-10.75	-10.82	-10.63
FAP13	HCl/NaCl	5.2	6.7	1542	0.7	43.3	24.2	6.3	-10.72	-10.73	-10.80
FAP14	HCl/NaCl	8.7	6.7	1537	0.7	27.6	11.8	3.5	-10.91	-11.05	-11.05
FAP15	HCl/NaCl	8.4	6.8	1557	0.7	27.7	12.5	4.5	-10.98	-11.09	-11.02
FAP16	HCl/NaCl	9	7	1516	0.6	32.7	18.4	7.9	-10.90	-10.91	-10.75
FAP17	NH_4OH/NH_4Cl	9.5	9.4	4477	4.2	21.9	11.6	8.0	-10.70	-10.73	-10.38
FAP18	NH_4OH/NH_4Cl	9.8	9.6	4754	3.8	22.9	11.3	8.8	-10.74	-10.81	-10.39
FAP19	NH_4OH/NH_4Cl	10.2	10.1	4590	4.2	13.3	4.7	10.3	-10.94	-11.15	-10.29
FAP20	NH_4OH/NH_4Cl	10.3	10.4	3886	2	19.0	8.6	11.4	-10.99	-11.14	-10.50
FAP21	NaOH/NaCl	11.7	11.4	4366	3.3	0.2	–	–	-11.53	–	–
FAP22	NaOH/NaCl	11.7	11.6	2677	3.5	0.2	–	–	-11.62	–	–

Table 2: Potential secondary phases and their solubility products considered in saturation state calculations.

Name	Abbreviation	Equation	Solubility product	Reference
Igneous fluorapatite	FAP	$Ca_{10}(PO_4)_6F = 10Ca^{2+} + 6PO_4^{3-} + 2F^-$	-118	Stumm and Morgan, 1996
Igneous hydroxyapatite	HAP	$Ca_{10}(PO_4)_6OH_2 = 10Ca^{2+} + 6PO_4^{3-} + 2OH^-$	-114	Stumm and Morgan, 1996
Fluorite		$CaF_2 = Ca^{2+} + 2F^-$	-10.04	Johnson et al., 2000
Portlandite		$Ca(OH)_2 + 2H^+ = Ca^{2+} + 2H_2O$	22.55	Johnson et al., 2000
Octa calcium phosphate	OCP	$Ca_8(HPO_4)_2(PO_4)_4,5H_2O = 8Ca^{2+} + 6PO_4^{3-} + 2H^+ + 5H_2O$	-93.8	Stumm and Morgan, 1996
β tri calcium phosphate	β-TCP	$Ca_3(PO_4)_2 + 2H^+ = 3Ca^{2+} + 2HPO_4^{2-}$	-7.96	Wagman et al., 1982
Di calcium phosphate anhydrous	DCPA	$CaHPO_4 = Ca^{2+} + HPO_4^{2-}$	-6.7	Wagman et al., 1982
Di calcium phosphate di hydrated	DCPD	$CaHPO_4,2H_2O = Ca^{2+} + HPO_4^{2-} + 2H_2O$	-6.6	Wagman et al., 1982

Table 3: Solution saturation of potential secondary products in steady-state outlet solutions of all of FAP dissolution experiments performed in the present study. Saturation indexes are calculated according to $\mathrm{Log}(\Omega) = \mathrm{Log}(Q/K_s)$ where Q designates the ionic activity product and K_s the solubility product of the considered solid. The reference provided under each value indicates the source of its solubility constant.

Phase	**pH**	**HAP**	**Fluorite**	**Portlandite**	**β-TCP**	**OCP**	**DCPA**	**DCPD**
Ref.		Stumm et Morgan, 1996	Johnson et al., 2000	Johnson et al., 2000	Wagman et al., 1982	Stumm et Morgan, 1996	Wagman et al., 1982	Wagman et al., 1982
FAP0	3.0	-61.5	-5.3	-20.9	-17.1	-56.9	-6.6	-6.7
FAP1	3.3	-45.1	-2.9	-19.6	-12.1	-43.1	-4.8	-4.9
FAP2	3.7	-47.3	-4.2	-19.3	-12.9	-46.1	-5.4	-5.5
FAP3	4.5	-40.1	-4.6	-17.9	-11.0	-41.5	-5.1	-5.2
FAP4	5.1	-33.1	-4.9	-16.9	-9.0	-36.6	-4.6	-4.7
FAP5	5.8	-30.9	-5.7	-16.0	-8.6	-36.2	-4.8	-4.9
FAP6	5.8	-33.0	-6.3	-16.1	-9.2	-38.1	-5.1	-5.2
FAP7	6.1	-28.3	-6.1	-15.4	-7.9	-34.7	-4.8	-4.9
FAP8	6.2	-27.3	-5.9	-15.3	-7.6	-34.0	-4.7	-4.8
FAP9	6.2	-25.1	-5.8	-15.1	-6.9	-32.1	-4.4	-4.5
FAP10	6.2	-17.5	-4.8	-14.6	-4.5	-25.5	-3.5	-3.6
FAP11	6.6	-14.3	-5.2	-14.0	-3.7	-23.7	-3.4	-3.5
FAP12	6.6	-13.1	-4.6	-13.8	-3.3	-22.7	-3.3	-3.4
FAP13	6.7	-12.5	-5.0	-13.8	-3.2	-22.2	-3.2	-3.3
FAP14	6.7	-16.0	-5.7	-13.9	-4.3	-25.4	-3.7	-3.8
FAP15	6.8	-13.9	-5.5	-13.6	-3.7	-24.0	-3.6	-3.7
FAP16	7.0	-10.4	-4.9	-13.2	-2.6	-21.3	-3.2	-3.3
FAP17	9.4	8.0	-5.1	-8.5	1.9	-12.2	-3.3	-3.4
FAP18	9.6	9.5	-5.0	-8.1	2.3	-11.5	-3.3	-3.4
FAP19	10.1	8.2	-5.1	-7.5	1.7	-14.0	-3.9	-4.0
FAP20	10.4	13.3	-4.8	-6.7	3.1	-10.5	-3.6	-3.7
FAP21	11.4	10.0	-8.2	-5.4	1.5	-16.5	-5.1	-5.2
FAP22	11.6	11.2	-8.2	-5.0	1.8	-16.1	-5.1	-5.2

Table 4: Chemical affinity of dissolution reaction ($A = -2.303RTLog\left(Q/K_s\right)$) in kJ/mol at steady-state conditions computed with respect to initial FAP with $Log(K_s)$=-118 (Stumm and Morgan, 1996) and with respect to the leached layer of di-calcium phosphate stoichiometry with $Log(K_s)$=-9.6 +/- 0.6 (Chaïrat et al., 2006 b).

Expt Number	FAP	leached layer
FAP0	158.8	21.1
FAP1	165.6	10.6
FAP2	187.1	14.1
FAP3	155.9	12.3
FAP4	123.6	9.5
FAP5	121.0	11.0
FAP6	135.7	12.6
FAP7	111.3	10.6
FAP8	105.9	10.2
FAP9	93.6	8.7
FAP10	47.0	3.3
FAP11	34.7	2.8
FAP12	25.3	2.2
FAP13	24.5	1.8
FAP14	47.4	4.6
FAP15	36.2	3.8
FAP16	15.4	1.9
FAP17	-62.0	2.3
FAP18	-69.2	2.3
FAP19	-57.7	5.9
FAP20	-83.3	4.1
FAP21	-37.3	12.3
FAP22	-42.3	12.8

Table 5: Results of open-system fluorapatite dissolution experiments performed in the present study at 25°C in presence of Ca, P, F enriched fluids at pH=3 and pH=9.9. $\mathrm{Log}(\Omega) = \mathrm{Log}\left(Q/K_s\right)$ represents the logarithm of solution saturation index with respect to the leached layer (see Chaïrat et al., 2006 b)

	Inlet solution concentrations						Outlet solution concentrations				
Ref.	**Ca**	**P**	**F**	**pH_{outlet}**	**S cm^2**	**flow rate**	**Ca**	**P**	**F**	**log (r_{Ca})**	**Log(Ω)***
		µmol/L				**$mg.s^{-1}$**		**µmol/L**		**mol. m^{-2} s^{-1}**	
FAP 23	6.0	0.0	0.0	9.77	4245.7	4.02	36.03	16.40	-	-10.55	-2.7
FAP 24	10.7	0.0	0.0	9.81	4243.2	4.01	33.83	13.90	4.30	-10.66	-2.8
FAP 25	0.6	0.0	0.0	9.86	4226.6	4.01	32.10	13.71	-	-10.74	-2.9
FAP 26	23.0	0.0	0.0	9.80	4225.0	4.06	68.90	-	-	-10.97	-
FAP 27	0.0	17.5	0.0	9.80	4250.6	4.10	29.93	35.00	-	-10.81	-2.3
FAP 28	0.0	35.1	0.0	9.70	4247.9	4.17	17.00	37.15	4.99	-10.87	-2.5
FAP 29	0.0	25.1	0.0	9.65	4246.6	4.16	16.43	36.90	3.49	-10.81	-2.5
FAP 30	0.0	37.4	0.0	9.75	4245.3	4.15	13.05	45.10	3.27	-10.85	-2.6
FAP 31	0.0	0.0	78.9	9.91	4234.9	3.88	23.90	0.00	87.30	-10.76	-3.0
FAP 32	0.0	0.0	121.1	9.84	4233.2	3.96	36.30	-	127.26	-10.83	-
FAP 33	0.0	0.0	73.7	9.80	4232.0	3.37	37.60	0.00	82.10	-10.87	-2.5
FAP34	81.8	0.0	0.0	3.02	115.4	73.78	131.60	30.10	10.10	-7.50	-3.1
FAP35	42.5	0.0	0.0	3.08	121.3	87.00	80.80	24.50	8.17	-7.54	-3.4
FAP36	21.8	0.0	0.0	3.02	484.3	77.58	83.36	35.09	14.25	-7.97	-3.3
FAP37	32.6	0.0	0.0	3.05	114.7	185.77	52.16	11.38	3.79	-7.51	-3.9
FAP38	14.3	0.0	0.0	3.10	119.8	79.02	181.30	21.75	7.25	-7.63	-3.0
FAP39	55.7	0.0	0.0	3.09	118.8	83.33	627.50	32.27	10.76	-7.32	-2.4
FAP40	2123.0	0.0	0.0	3.10	121.9	62.00	2192.00	21.42	7.14	-7.47	-2.1
FAP41	591.6	0.0	0.0	3.06	116.6	79.22	624.20	20.10	5.15	-7.64	-2.6
FAP42	0.0	20.8	0.0	3.05	116.6	147.83	17.51	32.06	3.50	-7.66	-3.9
FAP43	0.0	19.6	0.0	3.08	118.6	68.93	51.43	51.41	17.14	-7.52	-3.2
FAP44	0.0	222.5	0.0	3.09	115.7	82.17	37.43	247.10	7.49	-7.58	-2.7
FAP45	0.0	328.6	0.0	3.07	122.6	84.73	33.40	338.60	6.68	-7.64	-2.6
FAP46	0.0	714.8	0.0	3.09	115.6	81.67	29.90	740.10	5.98	-7.85	-2.3
FAP47	0.0	0.0	94.0	3.09	117.8	85.50	36.00	19.00	93.98	-7.51	-3.8
FAP48	0.0	0.0	360.4	3.10	123.3	98.67	21.45	12.70	316.00	-7.77	-4.2

*The reacting mineral has been shown to be constituted by the leached layer formed at FAP having a di-calcium phosphate ($CaHPO_4$) stoichiometry with $LogK_s$=-9.6 +/- 0.6 (Chaïrat et al., 2006 b).